Monitoring B_0 field drift due to changes in environment temperature in a low field permanent magnet based MRI scanner

THESIS

submitted in partial fulfillment of the
requirements for the degree of

BACHELOR OF SCIENCE
in
PHYSICS

Author :	Lisa van Leeuwen
Student ID :	1316710
Supervisor :	Prof. dr. A. G. Webb
2^{nd} corrector :	Prof. dr. ir. T. H. Oosterkamp

Leiden, The Netherlands, July 11, 2018

Monitoring B_0 field drift due to changes in environment temperature in a low field permanent magnet based MRI scanner

Lisa van Leeuwen

Huygens-Kamerlingh Onnes Laboratory, Leiden University
P.O. Box 9500, 2300 RA Leiden, The Netherlands

July 11, 2018

Abstract

In developing countries there is a high demand for medical diagnosis and treatment. A diagnosis is generally made with the aid of modern imaging techniques. However these techniques are very expensive and not available for the majority of people living in third world countries. For the diagnosis of hydrocephalus the requirements of the resolution of an image are not so high. We take the criteria to diagnose young children in developing countries suffering from hydrocephalus as the starting point of the development of a portable low field MRI scanner based on permanent magnets. We also have to take into account that temperature control might be poorly available or even absent in areas where the portable MRI will be used. In this bachelor research project we use measurements of the temporal stability and thermal stability of the Halbach magnet to show what the three-dimensional stability of the magnetic field looks like under temperature fluctuations. This data can be used to create a feedback loop that corrects for the magnetic field drift and eventually results in better image reconstruction.

Contents

Chapter 1

Introduction

By approximation hundreds of thousands of children in the south-eastern countries of the African continent are expected to be suffering from hydrocephalus, a condition in which cerebrospinal fluid is accumulated in the brain. The best way to diagnose hydrocephalus is by making use of MRI. MRI does not expose young children to harmful ionizing X-rays and the quality of the images is very high. Unfortunately MRI scanners are expensive, hence quite rare in developing countries. Not only are the initial costs, i.e. the purchase of the scanner, very high, but also the operating costs of the scanner are high. Another disadvantage of this powerful diagnostic technique is the fact that a very high magnetic field is required in order to create images. This need for a high magnetic field causes MRI scanners to be enormous machines, which are impossible to transport. This calls for a portable and more affordable way of MRI. An alternative for high field MRI is low field MRI, in which permanent magnets are used. Of course this technique also has its downsides. For example, the signal-to-noise ratio (SNR) is not as high as in high field MRI and the permanent magnets are more inhomogeneous than the magnets used in high field MRI. In this research project we will investigate the relation between changes of the temperature of the environment and the magnetic field and we will try to increase the data quality of low field MRI by using a feedback loop that corrects for this magnetic field drift.

Chapter 2

Theory

2.1 MRI

Magnetic Resonance Imaging, is a technique that allows us to make high resolution images of different types of tissue in the body. Images are created by the signals from hydrogen nuclei in the tissue, as MRI provides a spatial map of the protons[1]. Protons are charged particles with angular momentum P and magnetic moment μ and can therefor be thought of as a dipole. When a proton is placed in a strong magnetic field the spins will align at an angle of 54.7 ° with respect to the magnetic field B_0 (figure 2.1).

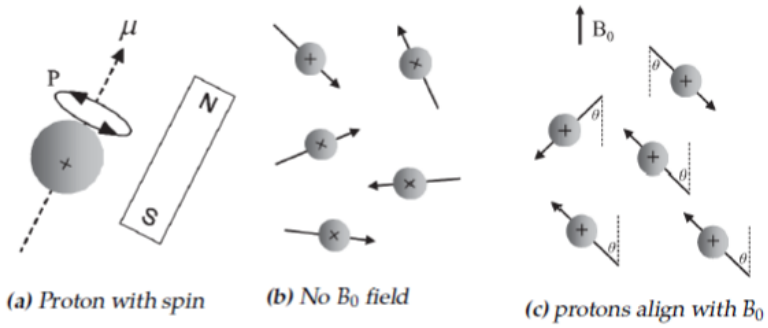

Figure 2.1: *The spins of theproton align at an angle of 54.7 ° with respect to the applied magnetic field B_0 [1].*

The spins can be either aligned parallel or anti-parallel. The confiuration in which the spins of the protons are aligned anti-parallel is the more favourable state, because the energy is lower. The MRI signal arises from the difference between the number of protons in the parallel and

anti-parallel configuration.

$$\frac{N_{\text{parallel}} - N_{\text{anti-parallel}}}{N_{\text{total}}} = \frac{\gamma h B_0}{4\pi k_{\text{B}} T}$$

with N the number of protons, γ the gyromagnetic ratio, k_{B} the Boltzman constant and T the temperature. When measuring a sample the MRI uses the net-magnetisation of the proton spins in that sample. The net-magnetisation is given by the following equation.

$$M_0 = \sum_{n=1}^{N_{\text{total}}} \mu_{\text{z,n}} = \frac{\gamma h}{4\pi}(N_{\text{parallel}} - N_{\text{anti-parallel}}) = \frac{\gamma^2 h^2 B_0 N_{\text{total}}}{16\pi^2 k_{\text{B}} T}$$

However, the net-magnetisation does not give us enough information to distinguish between different sorts of tissue. We can determine the tissue in the sample by measuring the relaxation times T_1 and T_2. To determine the relaxation times a RF pulse is applied, which adds energy to the system and disrupts the equilibrium. The relaxation time refers to the time the spin takes to return to equilibrium. The T_1 is the time the z-component takes to return to equilibrium and T_2 is the time the xy-component takes to return to equilibrium.

2.2 Low field MRI

The images made with a classical MRI (as described in the previous section) are of high quality and allow for precise diagnosis. Another advantage is that no harming radiation is used in this technique. Unfortunately a downside of classical MRI is that it is an expensive imaging technique, which makes it unsuitable for use in developing countries. That is why in this project we want to develop a portable and low-cost MRI scanner for the diagnosis of hydrocephalus. One of the most costly elements of classical MRI is the strong magnetic field generated by superconducting coils. We want to replace this way of generating a magnetic field by making use of permanent magnets. Our magnets are made of neodymium(a more detailed description of the magnets will be given in section 2.3). The magnets are arranged in a so-called Halbach array. The space between the four Halbach magnets rings is 2.5 cm (figure 2.2). A simulation of the magnetic field is also shown in figure 2.2.

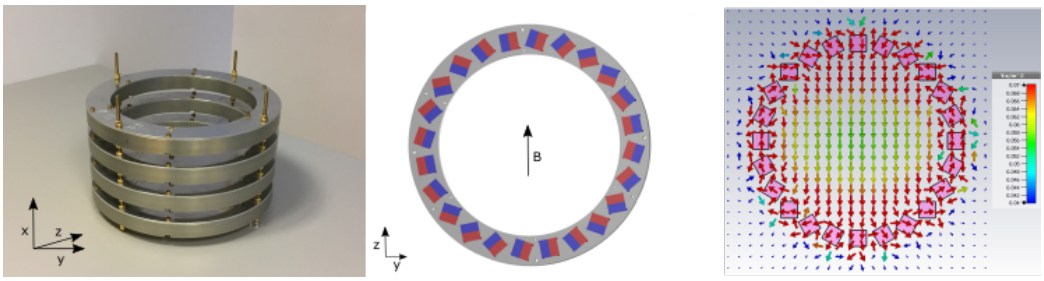

Figure 2.2: *The setup of the permanent magnet.* ***Left:*** *shows an image of the four Halbach magnet rings.* ***Middle:*** *shows the inside of one ring. The magnets are arranged in a Halbach aray configuration.* ***Right:*** *Simulation by Thomas O'Reilly of the magnetic field inside and outside the Halbach array. The length and colour of the arrows represent the strength of the field.*

2.3 Magnetization of the field

One of the main aspects of this project is to experimentally determine the relation between the magnetic field drift and temperature. In a 2015 paper by Cooley et al [2] it is shown that there is a magnetic field drift caused by temperature change. In figure 2.3 we see an image where on the left the temperature drift was not corrected for and on the right a temperature correction is implemented resulting in a sharper image.

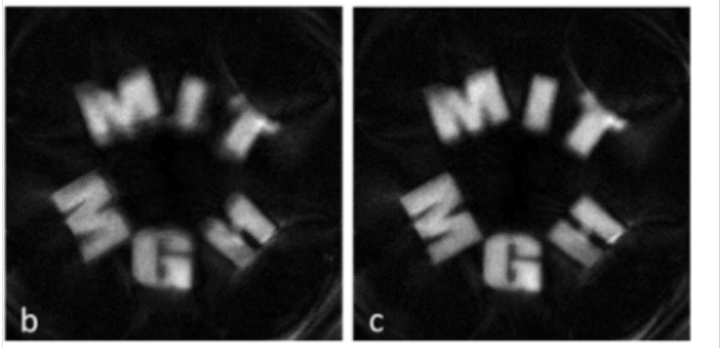

Figure 2.3: *Image from a paper by Cooley et al [2].* ***Left:*** *image where temperature drift is not corrected.* ***Right:*** *image where a temperature drift correction is implemented.*

Figure 2.5 shows the spontaneous magnetization of the magnet as a function of the fraction of the Curie temperature. Above this temperature materials irreversibly lose their permanent magnetic properties. The Curie temperature is a characteristic of the chosen material of the magnet.

However, this temperature can slightly differ for magnets of the same material by different manifacturers. Our magnets are neodymium-52 magnets, the strongest type of commercially available permanent magnets [3]. Neodymium magnets are alloys made of neodymium (a rare-earth element), iron and boron. Together they form a $Nd_2Fe_{14}B$ tetragonal crystalline structure [4], this is shown in figure 2.4.

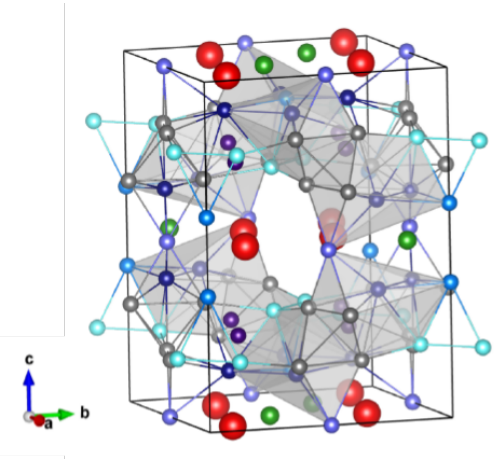

Figure 2.4: *Image from a paper by Takashi Miyake and Hisazumi Akai [5]. The $Nd_2Fe_{14}B$ tetragonal crystalline structure. The red balls represent neodymium, the green balls are boron and the other balls represent transition metals.*

The neodymium magnets owe their large magnetization and high Curie temperature to the iron in the crystalline structure [3]. The crystalline anisotropy, originating from spin-orbit coupling, is the reason for the magnetic anisotropy, which is a condition for a ferromagnet to be a permanent magnet material [5]. Neodymium magnets can be found in different grades, ranging from N-35 to N-52, where N denotes the Maximum Energy Product, the maximum strength that a material can be magnetized to. The different grades have slightly different Curie temperatures around 300 °C. Our measurement takes place at room temperature. Room temperature is considered a low temperature in this case as it is a small fraction of the Curie temperature. At low temperatures we can use the approximation that the magnetization of the field is linearly related to the temperature. In figure 2.5 we see that when the temperature increases, the magnetization decreases. Now this is what we have to show experimentally. However, not only the Curie temperature is important. Magnets have a characteristic maximum operating temperature above which a magnet will permanently lose a fraction of its magnetization. This temperature is

substantially lower than the Curie temperature, namely around 80°C for normal grades of neodymium magnets[6].

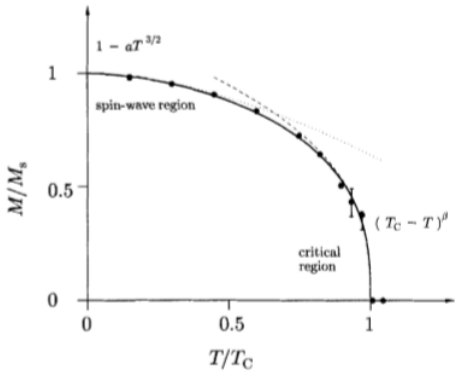

Figure 2.5: *The spontaneous magnetization of a ferromagnet as a function of temperature. This image is a copy from the book Magnetism in Condensed Matter by Blundell [7].*

2.4 Linear Hall sensors

To measure the magnetic field we will use linear Hall sensors. The principle behind the sensors is based on Halls original experiment [8]. In 1879 Edwin Hall discovered that a voltage perpendicular to the current I and the applied magnetic field B can be measured, and named this phenomenon the Hall effect. In figure 2.6 a Hall bar of thickness d is shown.

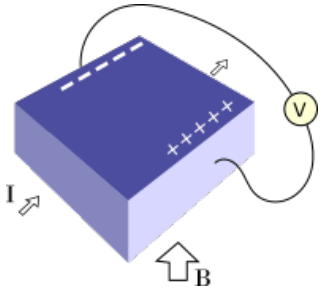

Figure 2.6: *Illustration of the experiment by Edwin Hall in 1879 [8]. The Hall voltage is perpendicular to both the current I and the magnetic field B. The voltage difference is shown on the Hall bar of thickness d.*

Because of the magnetic field the charges experience a force, the Lorentz force:

$$\vec{F} = q(\vec{v} \times \vec{B})$$

Because of this force the electrons in the sensor accumulate on one side creating a voltage difference. This quantity can be measured and is called the Hall voltage, which is related to the magnetic field B in the following way:

$$V_H = \frac{IB}{ned}$$

Here I is the current, n the density of mobile charges, e the charge of the carrier and d the thickness of the sensor. The sensor only measures the magnetic field in one direction.

2.5 Arduino

In this project we use Arduino boards to communicate with the linear Hall sensors and the temperature sensor. Arduino is an open source software and hardware company. The choice for Arduino boards is based on two of the advantages of Arduino. The first advantage coincides withone of the cornerstones of the project, namely that it should be available for everyone. Arduino itself is open access and large fragments of code written for and by the community are also readily and open access available. Another important aspect of the project is that the low field MRI should be low cost as it is meant for diagnosis in developing countries. Arduinos are relatively inexpensive making them a pre-eminently suitable hardware option for controlling the sensors. A downside of communication with Arduino is that the used language is C++, which is a very sensitive (and to some extent even capricious) language. This also makes it more difficult to detect the flaw when the data output seems to be incorrect.

Version of July 11, 2018– Created July 11, 2018 - 14:35

Chapter 3

Methods

In this chapter the setup of the experiment will be discussed in section 3.1. Also an important fragment of communication protocol between the linear Hall sensors and the Arduino-compatible micro-controller will be explained (section 3.2). Finally we will elaborate on the way we have altered the room temperature before and during the measurement in section 3.3.

3.1 The sensor arrays

We want to find a relation between the magnetic field drift and the temperature in the room. We could use this to correct for temperature fluctuations in a feedback loop, improving the data quality. In order to correct for the field drift it is necessary to measure the influence of temperature on the magnetic field. We build an array of linear Hall sensors (Infineon TLE4998S3) and a temperature sensor (SHT21 HTU21) on a cylinder that fits precisely around the bore. The importance of measuring as close to the magnet as possible becomes clear when looking at figure 2.2. A property of the Halbach array is the strong magnetic field drop off outside the magnet array. The further away from the magnet the weaker the field. It is undisirable to have a weak signal because the percentual field drift will be more inaccurate. The sensors are placed such that there is a large variation in position as well as to receive as much signal as possible. Between the magnet rings there is very little signal, so the sensors have to be placed on the heights of the rings (3.3 cm, 8.3 cm ,13.3 cm , 18.3 cm).

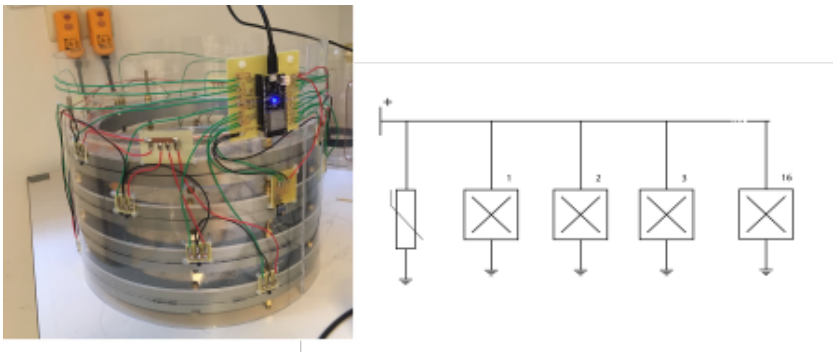

Figure 3.1: *The setup of the outer magnetic field sensor array.* ***Left:*** *shows an image of the plastic cylinder with the Hall sensors and the temperature sensor fixed to it.* ***Right:*** *shows a schematic drawing of the parallel circuit of the sensor array.*

To optimize the reception of the signal some sensors are slightly shifted upwards or downwards. In fact the exact positions of the sensors are not of great significance as their main purpose is to create a global overview of the behaviour of the magnetic field on the outside of the magnet. To find a relation between the behaviour of the magnetic field as a function of temperature on the outside and inside of the bore we also need to measure the field within the magnet.
For the inner array we use six sensors that can be placed in different configurations by using different gaps in the acryllic disk. This grid of gaps is made with a lasercutter. In the exact center of the magnet the magnetic field exceeds the range of the sensors, causing them to overload. Therefore they have to be placed in a setup just below the middle. The setup consists of an acrylic circular disk with laser printed gaps (figure 3.2). The size of the gaps are chosen to be precisely the size of one sensor in order to keep it firm in the right position.

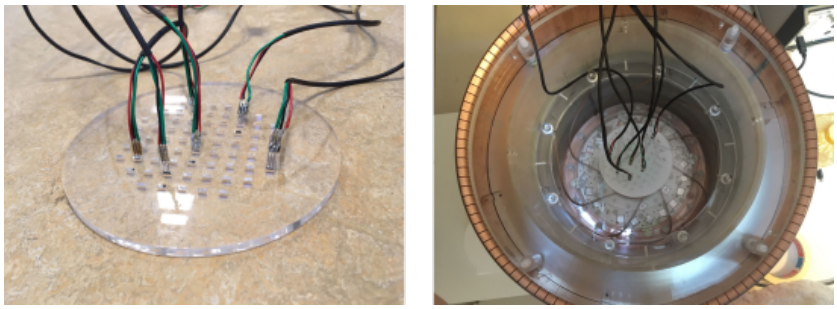

Figure 3.2: *The setup of the array of linear Hall sensors measuring the magnetic field within the bore.* ***Left:****The sensors are not fixed and can be placed in different gaps to measure the field on different positions.* ***Right:*** *The circular disk with sensors placed in the magnet.*

The sensors on the fixed outer array and the loose sensors within the bore are both connected in a parallel circuit (figure 3.1, right), one for the inner array and one for the outer. The third pin (the data pin) of each sensor is connected to an ESP32, an Arduino-compatible micro-controller with 16 PWM pins.

3.2 Data acquisition and the SENT protocol

We want to acquire data continuously in order to determine the stability of the magnetic field as a function of temperature. The linear Hall sensors make use of the Single Edge Nibble Transmission (SENT) protocol to communicate with the ESP32. Since there is no Arduino code readily available we have written the code by making use of the definition of the protocol in the data sheet of the TLE4998S3. As this project is part of a large open source project this code will eventually be made available as well. For now we will briefly explain the steps of the protocol (figure 3.3), however a more extended description can be found in the data sheet [9]. The protocol starts with a synchronization period of 168 μs followed by a 4 bit status nibble. The status nibble controls the functioning and the sensitivity (range) of the chip. After the status nibble two data packets, each consisting of three nibbles are transferred. The pulse length of the data nibbles is 108-243 μs. The first data packet contains the magnetic field data and the second data packet contains the temperature data of the sensor. However, we dot not use the temperature data of the linear Hall sensors. The final nibble is a CRC nibble. The data sheet contains an example code for CRC generationas which can be found in chapter 13 figure 15 of the data sheet [9] and in appendix A.

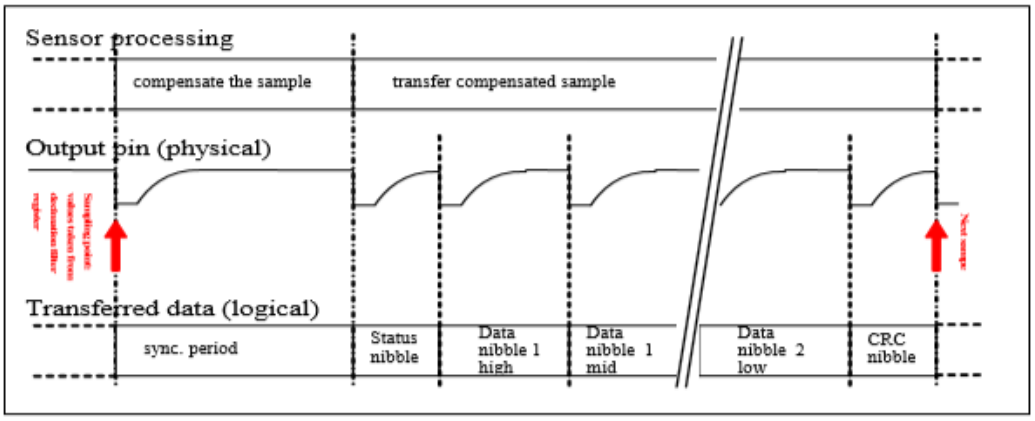

Figure 3.3: *Copy of the schematic overview of the SENT frame. The original figure is figure 13, which can be found in chapter 13 of the datasheet [9].*

3.3 Temperature control before and during the measurements

In order to show a relation between the field drift and the temperature we need a strong increase or decrease of the temperature throughout the measurement. To control and change the temperature in the lab we use the hospital's heat regulation system. Because of the feedback system of the thermostat the temperature decrease is more smooth than the temperature increase. This is shown in figure 3.4. During this project the measurements will be carried out only making use of temperature decrease.

That is why on the day of the measurement we raise the room temperature by raising the thermostat to the maximum. Because the lab in which the measurement takes place is relatively small, the temperature increases rather easily. Just before starting the measurement we lower the thermostat to the minimum value. The measurement takes place during the weekend to make sure the room remains locked and the temperature fluctuates as little as possible.

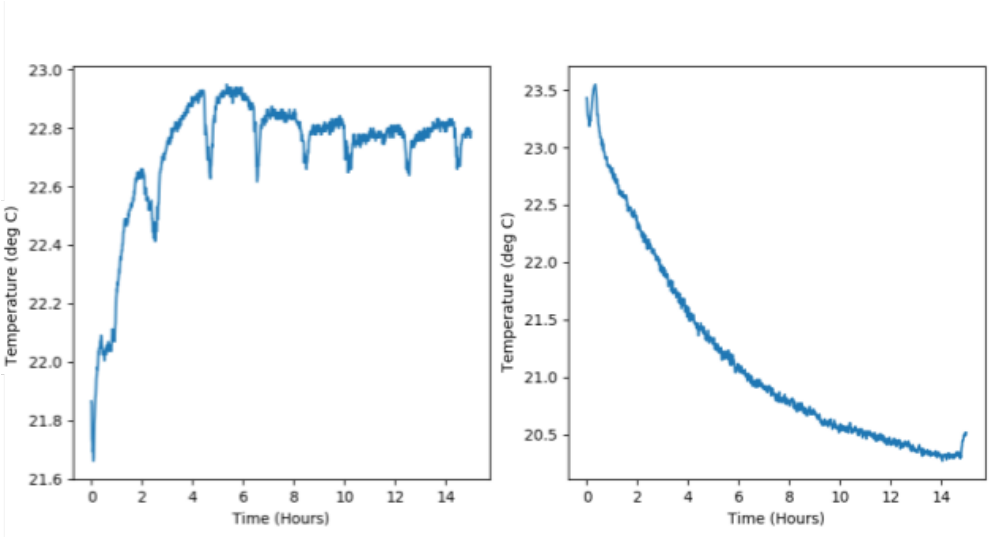

Figure 3.4: *Two measurements of the room temperature measured with the temperature sensor fixed on the cylinder around the bore.* ***Left:*** *displays the situation where the room was first cooled and then heated up, clearly showing the feedback system of the thermostat.* ***Right:*** *shows the situation where the room was first heated up and then cooled down.*

Chapter 4

Results

In this chapter we will look at the magnetic field measured by the linear hall sensors in the arrays. We start by looking at the behaviour of the temperature in the room as this is very important if we want to find a relation between the magnetic field. Then we will look at the results of the sensors on the inside of the bore and on the outside of the magnet rings. Figure 4.1 shows the decrease in room temperature during a sixty hour measurement which took place during the weekend.

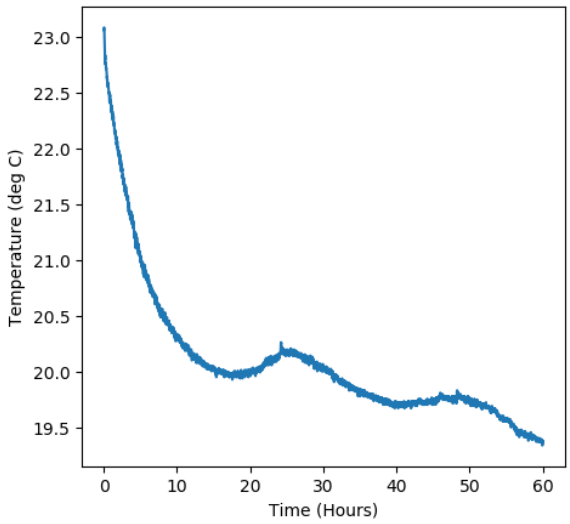

Figure 4.1: *Measurement of the room temperature in the lab during a sixty hour measurement.*

4.1 Results of the inner array sensors

In figure 4.2 we see the behaviour of the six sensors in the inner magnetic field array. A smoothing function written in Python is used as a low pass filter to eliminate noise from the dataset. When the sensor outputs a flawed data point due to an incorrect checksum that datapoint is stored as a NaN (Not a number) in the Python script. Also data points showing an increase or decrease of more than 0.1% compared to the previous valid data point are stored as NaNs. However Python does not allow us to carry out operations on the data with the NaNs, so the NaN values are finally substituted for the value of the previous data point of that sensor. The final operation is to replace every datapoint by the average of the datapoint before and after that datapoint.

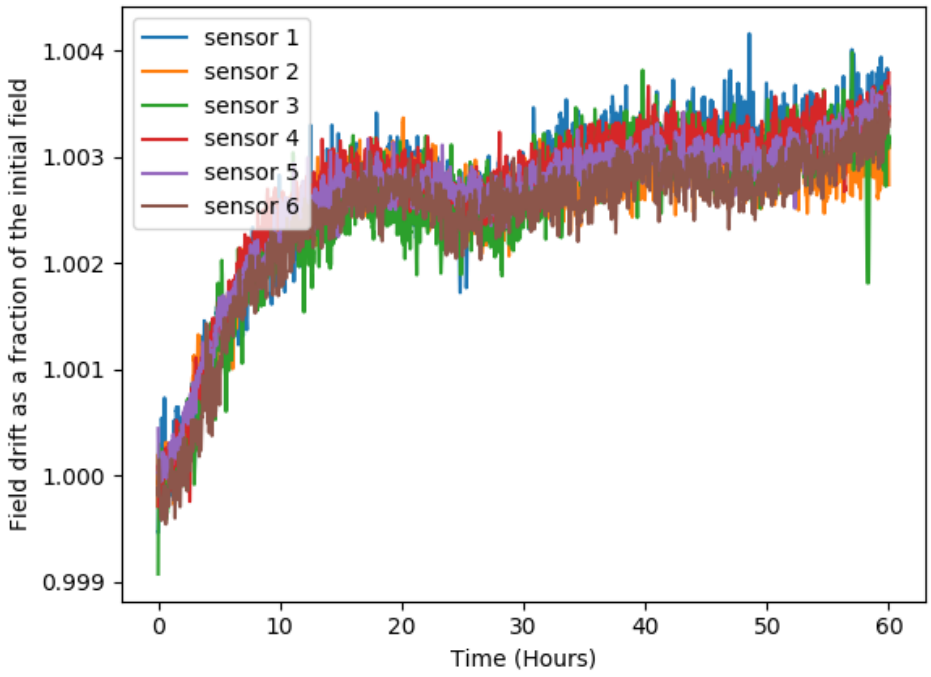

Figure 4.2: *The magnetic field drift in percentages of the six different sensors in the bore of the magnet during a sixty hour measurement. A smoothing function is applied on the dataset to eliminate noise.*

As we want to know the relation between the magnetic field and the temperature, we have plotted the field in the bore as a function of the room

Version of July 11, 2018– Created July 11, 2018 - 14:35

temperature in figure 4.3. Here we have used the smoothened data shown in figure 4.2. Since there is a strong correlation between the behaviour of the sensors in the bore we can take the average of each datapoint of the six sensors for further analysis. The correlation matrix of the six sensors is shown in appendix B figure B.1. Note that figure 4.3 is not chronological. The measurement started at around 23 °C and the room was then cooled. We have used a linear fit in Python to determine the slope of the linear relation. The slope of the line is equal to -0.0016. This is equal to a field drift of 0.16%.

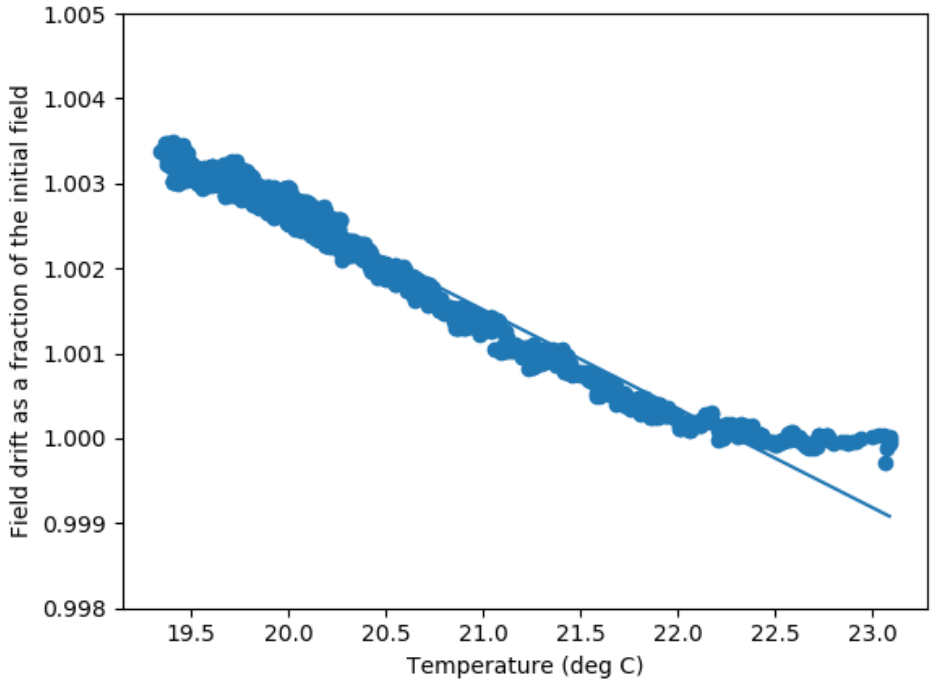

Figure 4.3: *The averaged magnetic field measured by the six different sensors in the bore of the magnet during a sixty hour measurement. A smoothing function was applied on the dataset. A linear fit through the data is also plotted in this figure. From around 22.2 °C to 23 °C the data points deviate from the linear fit.*

4.2 Results of the outer array sensors

In figure 4.4 we see the behaviour of the 16 sensors in the outer magnetic field array. We have used the same Python script to process and analyze the data as for the inner magnetic field array. From this figure we can

see that sensors 1,2 and 5 must have been defect during at least a part of the measurement. After this measurement the sensors have been replaced with new sensors. Sensor 5 now works well, but sensors 1 and 2 still exhibit the same behaviour.

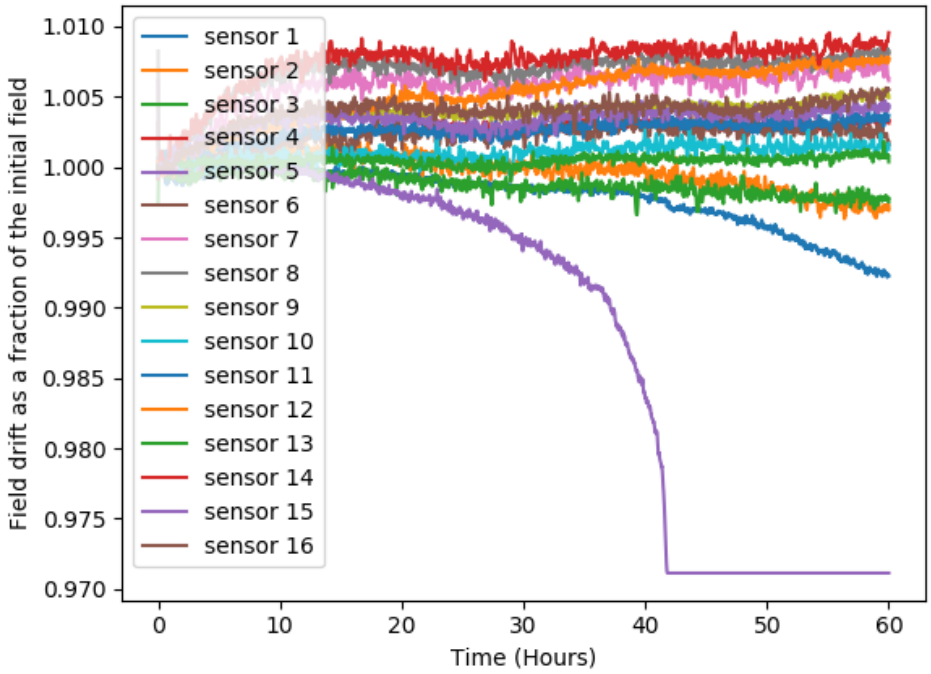

Figure 4.4: *The magnetic field drift in percentages of the 16 different sensors on the outside of the bore of the magnet during a sixty hour measurement. A smoothing function is applied on the dataset to eliminate noise.*

We want to know which sensors are reliable so in appendix B figure B.3 and figure B.4 you see the magnetic field drift as a function of temperature of all 16 sensors plotted individually with a linear fit included. The slopes of the fit are shown in table 4.1. The correlation between the 16 sensors is shown in B figure B.2.
We want to only include non-defect sensors in our analysis, therefore we have set a criterium for the behaviour of the sensors. From previous research [7] [2] and from the results of the inner magnetic field array we can see that there is a linear relation between the field drift and the temperature.

Based on this criterium the following sensors are excluded 1, 2, 3, 4, 5, 6, 10, 12 and 13. These slopes are also marked red in table 4.1.

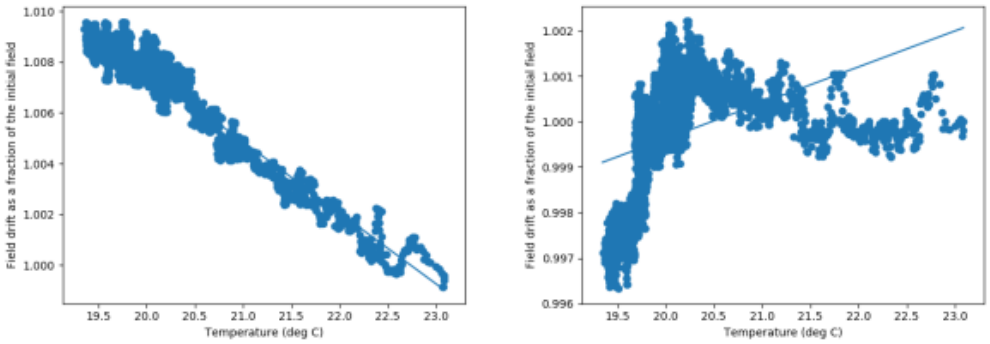

Figure 4.5: *Two measurements of the magnetic field drift as a function room temperature measured with the outer sensor array.* ***Left:*** *displays the data of sensor 14, one of the functioning sensors.* ***Right:*** *shows the data of sensor 2, a not working sensor.*

Table 4.1: *Sensors and the slopes of the linear fit.*

Sensor	Slope
1	0.00178
2	0.00079
3	0.00071
4	-0.00080
5	0.01168
6	-0.00111
7	-0.00232
8	-0.00258
9	- 0.00164
10	- 0.00055
11	- 0.00108
12	-0.00284
13	- 0.00019
14	-0.00279
15	-0.00124
16	- 0.00155

The data of the working sensors can now be avaraged as we did for the inner array sensors (figure 4.6). The slope of the linear fit is -0.0019. Without omitting the data from the disfunctional sensors the slope is -0.00023. This means a field drift of 0.2 % for the working sensors and a field drift of 0.02 % of all 16 sensor. The field drifts measured with all 16

sensors and the field drift of only the working sensors differ by a factor of ten. This makes sense, as there is a large variation in measured rates of changes so together they avarage out.

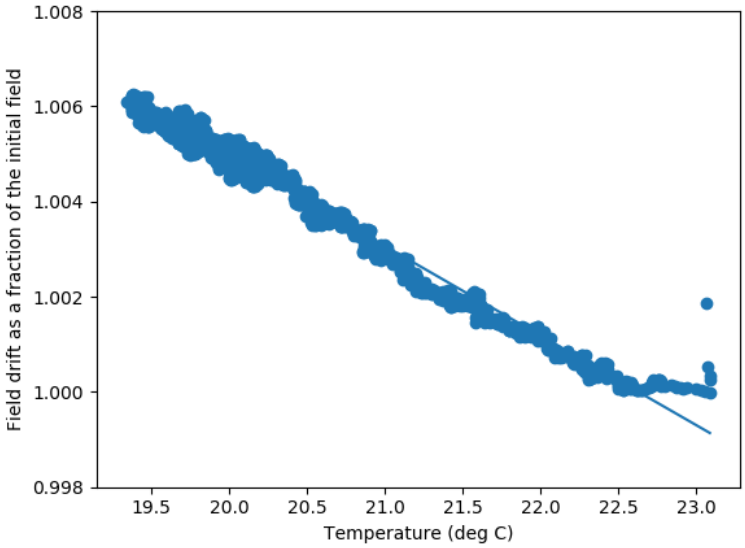

Figure 4.6: *The averaged magnetic field measured by the seven functioning sensors of the outer magnetic field array during a sixty hour measurement. A smoothing function was applied on the dataset. A linear fit through the data is also plotted in this figure.*

Chapter 5

Discussion

One of the main objectives of this research project was to find a relation between the change of temperature of the environment of the magnets and the behaviour of the magnetic field.
Figure 4.3 is the most important figure if we want to determine the relation between the magnetic field drift and the temperature measured in the lab. We see that the first part of the curve from about 19.5°C to 22°C shows a linear relation between the field drift (in percentages) and the temperature. The slope is -0.0016, which is 0.1% so 2.6 kHz per °C. This is not exactly the same as the field drift measured by Cooley et al [2] but this could be due to the magnets used in the Halbach array. Magnets from a different manufacturer can have a slightly different Curie Temperature and therefore have a different magnetization. However, from 22 °C to 23 °C the field drift shows a different behaviour. When looking at figure 4.2 and 4.1 this can be explained. The second part of figure 4.3 roughly corresponds to the first 5 hours of the measurement. Here we see that the temperature decrease is the strongest. On the other hand the part of figure 4.3 where there is a linear relation, corresponds to the entire measurement minus the first 5 hours. Here the temperature fluctuations are not as strong as in the first 5 hours. An explanation for the non-linear behaviour of the magnetic field drift could be that the magnets do not instantaneously respond to the change of temperature in the room. In that sense we can say there is a delay between the decrease of the room temperature and the change of strength of the magnetic field. It could be interesting to investigate if this inertia is also visible when we heat the room in a very short period of time instead of cooling the room.
When looking at figure 4.4, figure B.3 and B.4 we can tell that the sensors of the outer array are not as reliable as the sensors of the inner array. The

slope of the linear fit through the average of the magnetic field drifts as a function of temperature of the 16 sensors is -0.00023, which is a factor of ten smaller than the slope of the data on the inside of the bore. When we omit the data of the disfunctional sensors on the outside the slope becomes -0.0019, which is a lot closer to the slope measured on the inside. Furthermore according to the correlation array B.2 some of the sensors of the outer array are anticorrelated. An explanation for this phenomenon could be that the magnetic field is rapidly changing in magnitude and direction right outside the magnet ring. From figure 2.2 it is clear that the arrows representing the magnetic field point in different directions and have different magnitudes. Measuring the magnetic field slightly further away could be a solution. However a property of the Halbach array is that the field drops off rather fast further away from the magnet. The minimum changes we can measure in the field then are a higher percentage of the field, making the field drift data less accurate. For now it does not seem feasible to accurately predict the field drift on the inside of the bore based on the the field drift on the outside of the bore.
Another aim for this project was to use the relation between the magnetic field drift and the temperature in a feedback loop to improve image reconstruction. The importance of an implemented correction for the field drift caused by change of environment temperature becomes clear when looking at figure 5.1. The simulation on the left shows the LUMC phantom in a magnetic field with a field drift of 4 kHz as measured in our experiment. When we start working with a magnet with an even more homogeneous magnetic field (due to shimming) the influence of the field drift becomes larger due to spatial variation. In that case (middle simulation of figure 5.1 the LUMC phantom is barely recognizable.

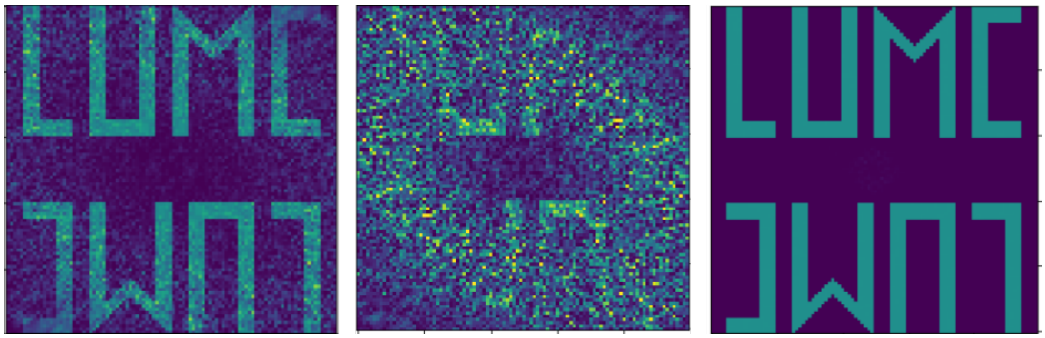

Figure 5.1: *Three simulations of a phantom in our magnetic field by Thomas O'Reilly.* ***Left:*** *shows the LUMC phantom in a magnetic field with a field drift of 4 kHz as measured in our experiment.* ***Middle:*** *shows the LUMC phantom in a magnetic field with a field drift of 25 kHz. This would be the case if the field becomes more homogeneous since a small change in frequency translates to a larger change in position.* ***Right:*** *shows the LUMC phantom after field drift corrections have been implemented.*

Unfortunately this was a relatively short research project and we have dealt with inconveniences to different extents. For example it is useful to keep in mind that the pins of the sensors are very fragile. When they break, the code will only output peculiar data but it will not stop working, which makes it harder to detect the actual cause of the flawed data.
However, we have shown a strong correlation between with the temperature of the environment and the change in magnetic field. The next step will be to integrate this in to image reconstruction.

Chapter 6

Conclusion and future prospects

We have confirmed that the change of temperature causes a linear drift in the magnetic field within the magnet bore, which is in agreement with the theory and with previous research [2]. In addition we have found that when the temperature decrease does not take place in a short period of time, the response of the magnetic field is not delayed and behaves as predicted. We know the magnetic field drift is equal to 2 kHz per °C and it would be very useful to implement this knowledge in the feedback loop.
Unfortunately we will have to find a different way to characterize the magnetic field as a function of temperature on the outside of the magnet because the outer sensor array is not reliable enough.
In a future project it would be useful to determine how rapidly the magnetic field adapts to temperature fluctuations to also account for that in a feedback loop, because we can not ignore the fact that when the temperature changes rapidly, the magnetic field drift is delayed and behaves differently. As soon as we have a model that can predict the magnetic field as a function of temperature we can test this model and the feedback loop by for example heating up the magnet locally, as this could potentially represent an actual situation.

Acknowledgements

I would like to use this section to thank the following people:

Andrew Webb, my supervisor during this bachelor research project. Thomas O'Reilly and Roel Burgwal for their patience, advice and guidance and of course for their motivational support especially during the countless programming crises. Tjerk Oosterkamp, the second corrector of this thesis. Wouter Teeuwisse for his counseling in the lab and clever practical solutions. Jaimy Plugge, my fellow bachelor project colleague in the lab for always being in good spirits and forr helping with numerous silly complications.

Appendix A

Checksum example code

```
// Fast way for any µC with low memory and compute capabilities
char Data[8] = {...};  // contains the input data (status nibble, 6 data nibble, CRC)
// required variables and LUT
char CheckSum, i;
char CrcLookup[16] = {0, 13, 7, 10, 14, 3, 9, 4, 1, 12, 6, 11, 15, 2, 8, 5};
CheckSum= 5; // initialize checksum with seed "0101"
for (i=0; i<7; i++) {
   CheckSum = CheckSum ^ Data[i];
   CheckSum = CrcLookup[CheckSum];
}
; // finally check if Data [7] is equal to CheckSum
```

Figure A.1: *Example code for checksum calculations as given in the data sheet [9] of the linear Hall sensors.*

Appendix B

Correlations

	0	1	2	3	4	5
0	1	0.786587	0.802315	0.837745	0.837885	0.817316
1	0.786587	1	0.768354	0.82366	0.826814	0.812687
2	0.802315	0.768354	1	0.819472	0.824953	0.802242
3	0.837745	0.82366	0.819472	1	0.870297	0.854602
4	0.837885	0.826814	0.824953	0.870297	1	0.857943
5	0.817316	0.812687	0.802242	0.854602	0.857943	1

Figure B.1: *Correlation array for the six sensors in the inner magnetic field array. The colours represent the strength of correlation between each two sensors.*

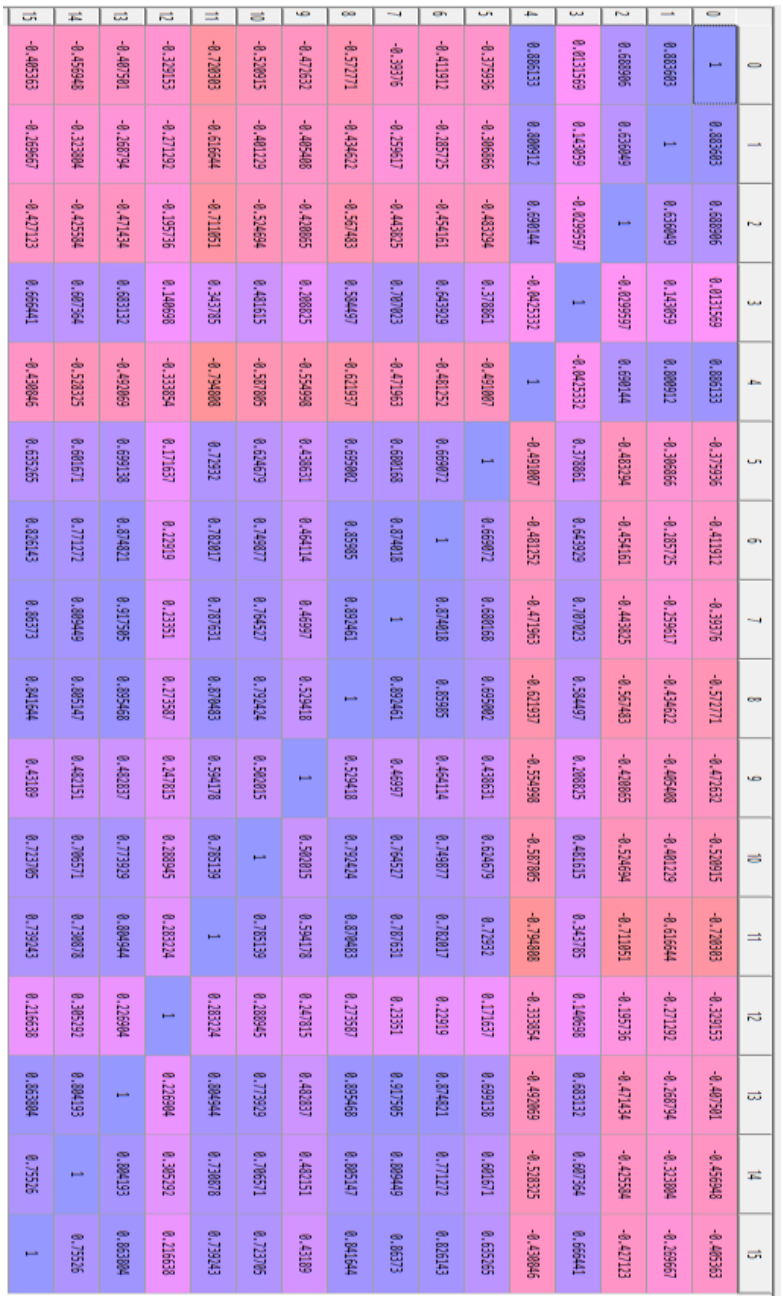

Figure B.2: *Correlation array for the 16 sensors in the inner magnetic field array. The colours represent the strength of correlation between each two sensors.*

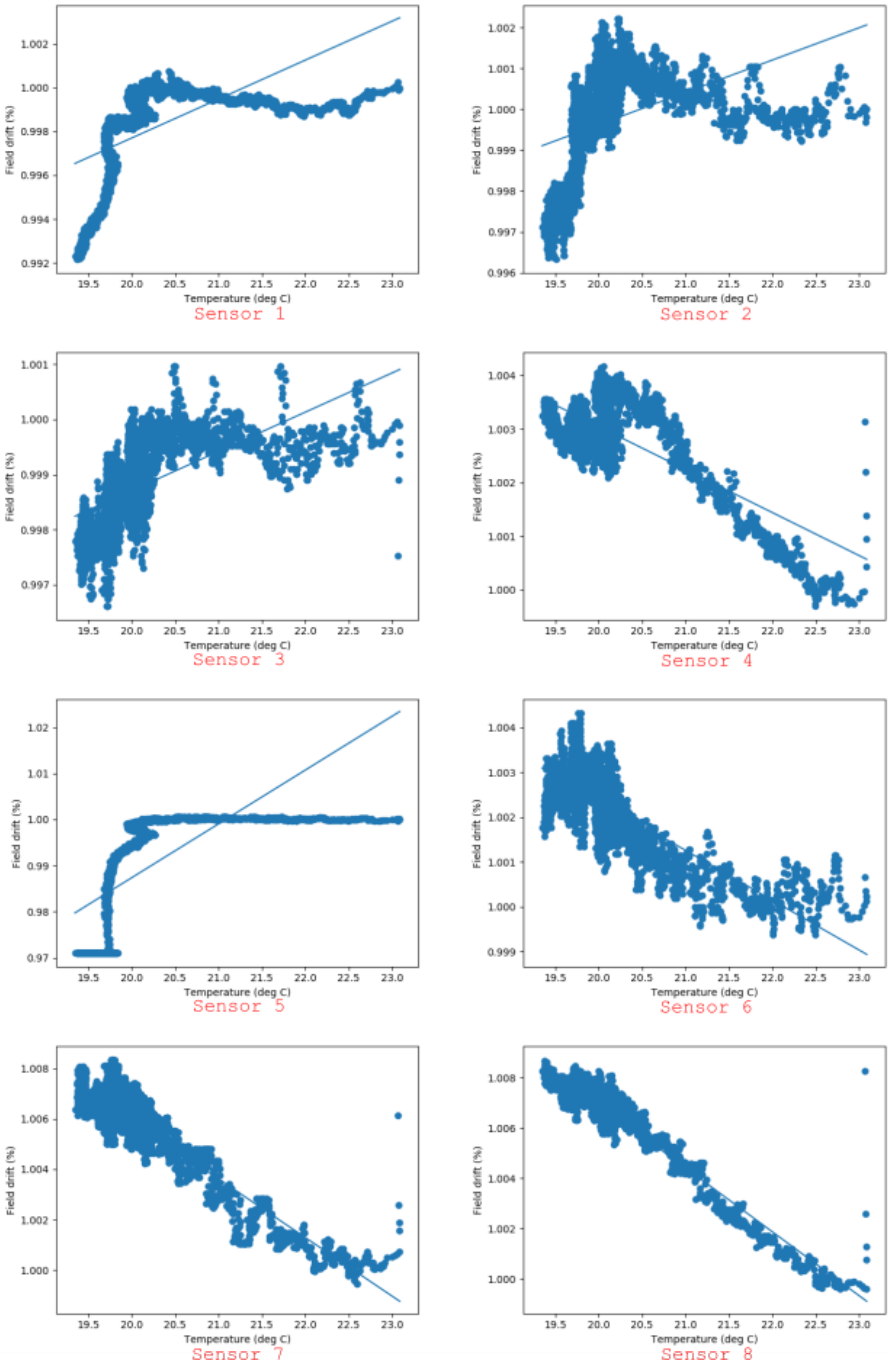

Figure B.3: *The magnetic field measured by the first eight sensors on the outside of the magnet during a sixty hour measurement. A smoothing function was applied on the dataset. A linear fit through the data is also plotted in this figure.*

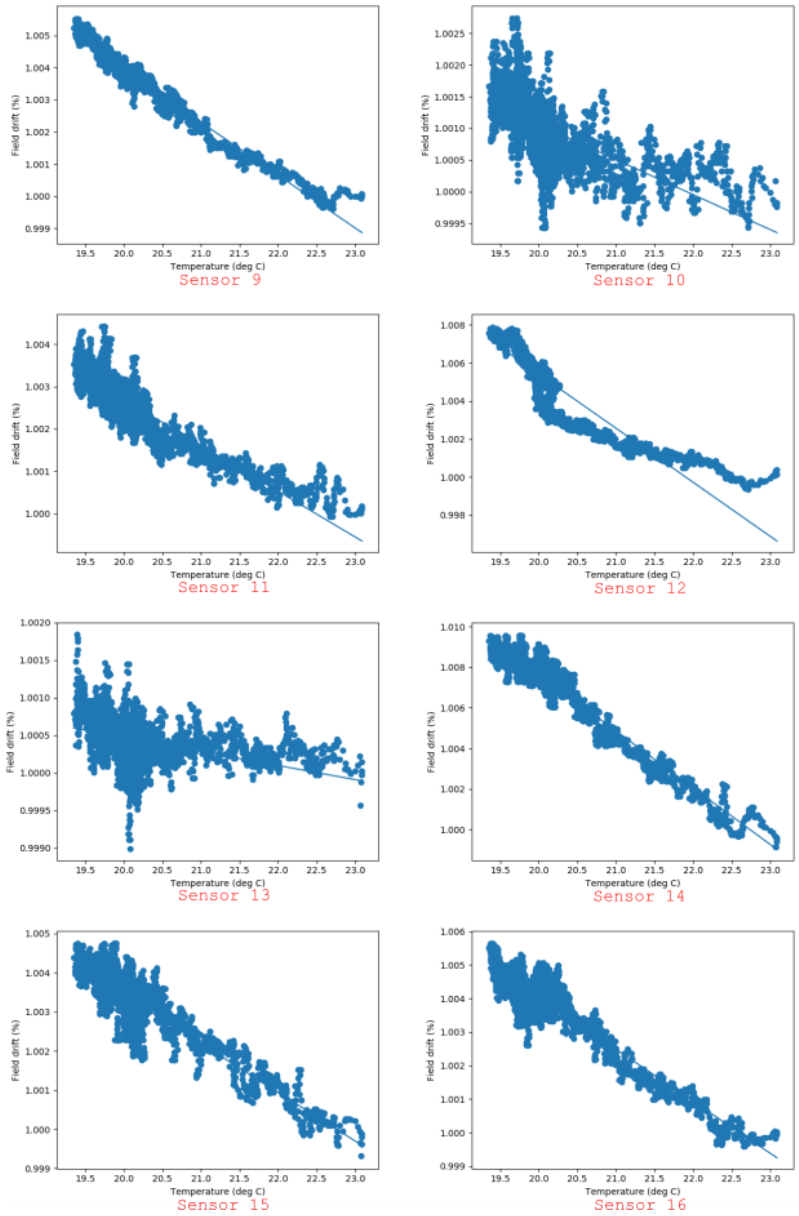

Figure B.4: *The magnetic field measured by the last eight sensors on the outside of the magnet during a sixty hour measurement. A smoothing function was applied on the dataset. A linear fit through the data is also plotted in this figure*

Bibliography

[1] N. B. Smith and A. Webb, *Introduction to Medical Imaging*, Cambridge University Press, 2011.

[2] C. Z. Cooley, J. P. Stockmann, B. D. Armstrong, M. Sarracanie, M. H. Lev, M. S. Rosen, and L. L. Wald, *Two-dimensional imaging in a lightweight portable MRI scanner without gradient coils: Lightweight MRI Scanner without Gradient Coils*, Magnetic Resonance in Medicine **73**, 872 (2015).

[3] T. Hinomura, S. Nasu, H. Kanekiyo, M. Uehara, and S. Hirosawa, *Magnetic Properties of Nd-Fe-B-Cr Nanocrystalline Composite Magnets*, Materials Transactions, JIM (1997).

[4] J. Fraden, *Handbook of Modern Sensors: Physics, Designs and Applications*, Springer, USA, 2010.

[5] T. Miyake and H. Akai, *Quantum Theory of Rare-Eart Magnets*, Journal of the Physical Society of Japan (2018).

[6] *KJ Magnetics FAQ*, `https://www.kjmagnetics.com/faq.asp`, Accessed: 2018-07-11.

[7] S. Blundell, *Magnetism in Condensed Matter*, Oxford University Press, New York, New York, 2001.

[8] S. H. Simon, *The Oxford Solid State Basics*, Oxford University Press, New York, New York, 2013.

[9] I. T. AG, *TLE4998S3 TLE4998S4 Programmable Linear Hall Sensor Data Sheet*, 2008-07 edition, 2008.